Materials Chemistry Horizons

RESEARCH

Efficacious Remediation of Methylene Blue (MB) and Crystal Violet (CV) from Aquatic Environment Using Magnetic Hydrogel Halloysite Nanotubes

Leila Choopani [a], Mohammad Mehdi Salehi [a], Reza Eivazzadeh-Keihan [a,*], Ali Maleki [a,*]

[a] Catalysts and Organic Synthesis Research Laboratory, Department of Chemistry, Iran University of Science and Technology, Tehran 16846-13114, Iran

***Corresponding author**: reza_eivazzadeh@alumni.iust.ac.ir (R. Eivazzadeh-Keihan); maleki@iust.ac.ir (A. Maleki)

Mater. Chem. Horizons, 2025, 4(1), 29-48 10.22128/mch.2026.3080.1069 OPEN ACCESS

ABSTRACT

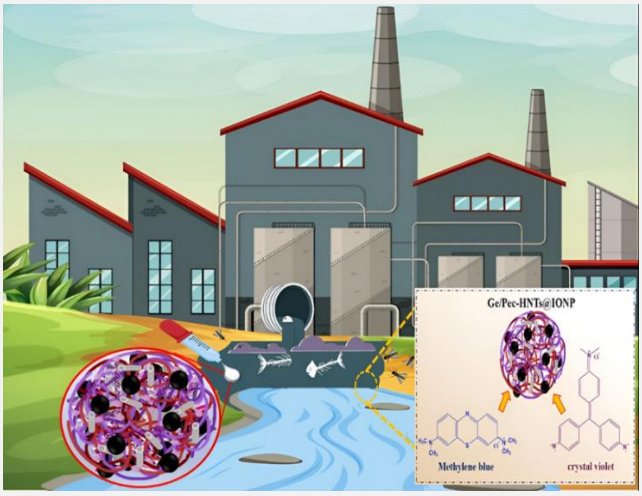

A magnetic gelatin/pectin halloysite nanotube composite (Ge/Pec-HNTs@IONP) was synthesized via a two-step process. First, a gelatin/pectin (Ge/Pec) hydrogel was fabricated and crosslinked with glutaraldehyde. Subsequently, halloysite nanotubes (HNTs) were incorporated, and the composite was magnetized in situ by embedding iron oxide nanoparticles (IONPs) to yield the final Ge/Pec-HNTs@IONP magnetic hydrogel.The physicochemical properties of the synthesized adsorbent were characterized using several analytical techniques: FT-IR, XRD, FE-SEM, EDX, TGA, VSM, and BET surface area analysis. The BET results indicated a surface area of 35.244 $m^2 \cdot g^{-1}$, a pore volume of 0.0690 $cm^3 \cdot g^{-1}$, and an average pore size of 7.83 nm. VSM analysis confirmed its magnetic properties with a saturation magnetization of 14.51 $emu \cdot g^{-1}$. TGA demonstrated good thermal stability, with approximately 78% of the mass retained up to 600 °C.The adsorption efficiency of the Ge/Pec-HNTs@IONP composite was evaluated for the removal of cationic dyes, Methylene Blue (MB) and Crystal Violet (CV), from aqueous solutions. Key operational parameters, including solution pH (4–10), adsorbent dosage (0.003–0.03 g), contact time (5–30 min), and initial dye concentration (25–150 $mg \cdot L^{-1}$), were systematically investigated to optimize the process.The adsorption isotherm data were best described by the Freundlich model, indicating multilayer adsorption on a heterogeneous surface. Kinetic studies revealed that the adsorption process followed a pseudo-second-order (PSO) model for both dyes, suggesting chemisorption as the dominant mechanism. Furthermore, the composite demonstrated excellent reusability, maintaining its adsorption capacity without significant loss over three consecutive adsorption-desorption cycles under optimal conditions.

Keywords: Wastewater treatment, methylene blue, crystal violet, pectin, gelatin

1. Introduction

Over the past few years, industrial pressure has increased dramatically due to global population growth and technological development [1,2]. The textile industry, in particular, faces significant challenges in meeting the rising demand for fabrics [3]. Across multiple sectors, including textiles [5], cosmetics [6], plastics [7], and paper [8], synthetic dyes are heavily utilized to impart colour to finished products [4]. The effluents from these industries contain significant concentrations of dyes, which require treatment before discharge [8]. Notably, approximately 15% of the dyes used in industrial processes are released into the environment [9].

Common textile dyes such as methyl orange (MO) [10], Rhodamine B (RhB) [11], methylene blue (MB) [12,13], Congo red (CR) [14], crystal violet (CV) [15,16], Safranin-O [17], and Reactive Black-5 (RB5) [18] can be classified as neutral or cationic based on their specific chemical properties [19]. Many of these dyes, particularly aromatic organic compounds like MB, are highly stable, toxic, and pose serious health risks to humans, including nausea,

Received: September 30, 2025
Received in revised: October 30, 2025
Accepted: January 20, 2026

vomiting, tissue necrosis, and neurological damage [20,21]. Dyes such as CV are not only common industrial pollutants but are also known to have teratogenic, carcinogenic, and mutagenic effects, making their environmental release both hazardous and illegal [20,22]. Consequently, there is an urgent need to develop efficient processes for treating wastewater contaminated with MB and CV (chemical structures shown in **Figure S1**).

Several techniques have been developed for water decolorization and dye removal from industrial effluents. These methods include coagulation [23,24], photodegradation [25], chemical oxidation [26], flocculation [27], electrodialysis [28], membrane filtration [29], and adsorption [30,31]. Among these, adsorption stands out due to its simplicity, eco-friendliness, high efficiency, and cost-effectiveness for removing toxic dyes [32]. While other methods are effective, they often suffer from drawbacks such as high operational costs, significant energy consumption, and the generation of concentrated sludge, limiting their large-scale practicality [33,34]. Adsorption, by contrast, offers enhanced efficacy, selectivity, ease of recovery, and overall economic viability for contaminant removal [35,36].

Various adsorbents have been explored for this purpose, including porous materials [35,36], bioadsorbents [37], carbon nanotubes [38], metal-organic frameworks (MOFs) [39], and polymer-based systems [40,41]. Recently, researchers have focused on naturally occurring biopolymers, such as cellulose [49], gelatin [50], chitosan [51], pectin [52], alginate [53], and xanthan gum [54], due to their unique advantages, including non-toxicity [43], low production cost [44], biodegradability [45,46], and favorable adsorption properties [47,48]. Hydrogels, which are three-dimensional (3D) crosslinked polymeric networks, are particularly effective because their abundant functional groups can directly interact with and entrap pollutant molecules [55–57].

Gelatin (Ge), a bio-based protein derived from animal skin, bones, and connective tissues [58,59], is widely used in food, pharmaceutical, and chemical engineering industries due to its low cost, biocompatibility, and biodegradability [60–63]. Its abundance of hydroxyl, carboxyl, and amino groups allows for easy gelation and functionalization [64–66], making it an excellent base material for constructing 3D hydrogel structures [67,68]. Pectin (Pec), commonly extracted from apple pomace and citrus peels [69–71], is another promising biopolymer used in food, pharmaceutical, and chemical applications. It can be crosslinked with gelatin via glutaraldehyde, forming imine bonds between aldehyde and amine groups to create stable hybrid hydrogels [72,73]. Pec possesses numerous electron-rich functional groups (e.g., carboxyl, hydroxyl, acylamino) that enable strong electrostatic interactions with metal ions and organic cations, enhancing its suitability for adsorption applications [76,77]. Beyond adsorption, Pec-based materials are utilized in tissue engineering [78,79], drug delivery systems [80,81], pharmaceuticals [82,83], food industries [84,85], biomedical devices [85], contact lens manufacturing [86], and photography [87].

To improve the performance of biopolymer-based adsorbents, researchers often incorporate functional nanomaterials. Magnetic nanocomposites, for instance, facilitate easy separation from treated water using an external magnet. However, they can suffer from drawbacks such as poor mechanical strength [90], low adsorption efficiency [91], and difficult processability when combined with natural materials [92]. Incorporating iron oxide nanoparticles (IONPs) into hydrogels can enhance their mechanical and thermal strength, adsorption capacity, and separability [97–99]. Similarly, porous minerals like halloysite nanotubes (HNTs), a naturally occurring aluminosilicate from the kaolinite group [103,104], are attractive due to their low cost, high surface area, porosity, cation exchange capacity, and stability [105,106]. HNTs have been extensively studied for contaminant removal because of their unique tubular structure, high absorbability, and excellent stability [107,108]. Previous studies have demonstrated the effectiveness of HNT-based composites for dye adsorption. For example, Sadia Ata et al. reported a 98.7% removal of methylene blue using a halloysite-based hydrogel film within 30 minutes [110]. Lei Li et al. developed magnetic nonwovens with HNTs and IONPs for efficient heavy metal ion adsorption [111]. Selcan Erdem et al. achieved 88.3% tetracycline removal using halloysite-chitosan-alginate composites [112]. E. Türkeş et al. reported 83.9% MB adsorption using magnetic halloysite-chitosan nanocomposites [113].

Building on these advances, this study aims to develop a novel multifunctional adsorbent by integrating HNTs as a porous mineral, IONPs as a magnetic component, and a Pec/Ge biopolymer hydrogel matrix. The formulated composite, designated "Ge/Pec-HNTs@IONP," is fabricated by first preparing a Ge/Pec hydrogel crosslinked with glutaraldehyde, then incorporating HNTs, and finally performing in-situ magnetization to embed IONPs. This design is intended to enhance the specific surface area, porosity, and functional group density of the adsorbent. The resulting Ge/Pec-HNTs@IONP magnetic hydrogel halloysite nanotubes are expected to exhibit superior adsorption

performance for cationic dyes like MB and CV from aqueous solutions, offering a promising solution for efficient wastewater treatment.

2.Experimental

2.1. Materials and apparatus

Table S1. and **Table S2.** represent the materials, i.e., reagents, solvents, and instruments utilized in this study.

2.2. The Ge/Pec-HNTs@IONP magnetic hydrogel halloysite nanotubes

2.2.1. Preparation of Ge/Pec Hydrogel

The Pec solution was stirred continuously for an hour at room temperature (r.t.), adding 3.00 g of Pec to 50 mL of distilled water (d.w.). To make 3.00 g of a Ge solution, the powdered Ge was dissolved in 40 mL of d.w. at 40°C with continuous stirring for an hour. The Ge and Pec solutions were combined and agitated for two hours at r.t.. To crosslink the Pec and Ge, 0.94 mL (1.0 g) of glutaraldehyde was added to the solution drop-by-drop and incorporated into the mixture. The mixture was then agitated for two hours at r.t. to achieve homogeneity.

2.2.2. Preparation of Ge/Pec-HNTs@IONP magnetic hydrogel halloysite nanotubes

First, 10 mL of d.w. was used to evenly distribute 0.198 g of HNTs. The Ge/Pec hydrogel solution is then combined with the HNTs solution and stirred for 15 minutes. 40 mL of d.w. is used to dissolve the metal ions $FeCl_3.6H_2O$ (2.425 g) and $FeCl_2.4H_2O$ (1.1 g) before adding Ge/Pec-HNTs to the hydrogel. N_2 atmosphere was employed once the mixture's temperature was stirring 70°C. A dark solution (Ge/Pec-HNTs@IONP) was produced by adding ammonia solution (8 $mol.L^{-1}$, 20 mL) to the combination. 1.5 hours were spent stirring the final nanocomposite. The Ge/Pec-HNTs@IONP magnetic hydrogel halloysite nanotubes' black residue was rinsed with d.w. then, we used an external magnet to separate it numerous times. The magnetic hydrogel halloysite nanotubes were dried at the Owen for six hours at 65°C. The pathway preparation of Ge/Pec-HNTs@IONP magnetic hydrogel halloysite nanotubes is illustrated in **Figure 1.**

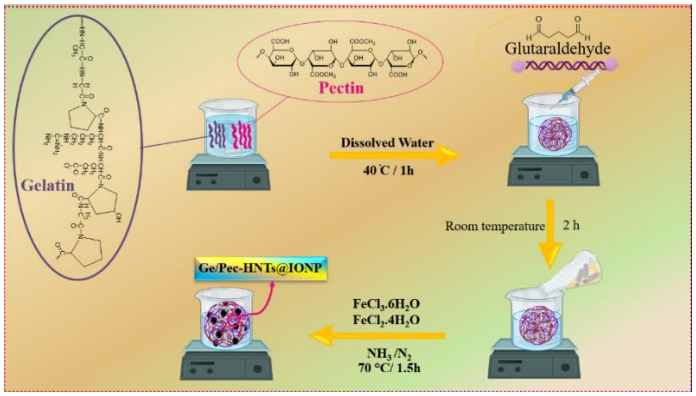

Figure 1. Schematic illustration of Ge/Pec-HNTs@IONP magnetic hydrogel halloysite nanotube preparation.

2.3. Batch adsorption experiments

Several tests included investigations on the Ge/Pec-HNTs@IONP magnetic hydrogel halloysite nanotubes' capacity to absorb MB and CV from aqueous environments. The effect of several parameters, for instance, pH, adsorbent dose, Duration time, initial concentration of MB and CV, and absorption time, were evaluated on the surface adsorption process. The pH was adjusted to a range of 2-10, using 1.0 M sodium hydroxide (NaOH) and 1.0 M hydrochloric acid (HCl) solutions. Different dosages of the nanocomposite hydrogel range from 0.003-0.03 g, with a duration of 5-30 min. and the initial MB and CV concentrations of 25-150 ppm for the best absorption conditions. Furthermore, different models of equilibrium adsorption isotherms, such as Langmuir and Freundlich, were studied ,and the relevant constants were determined. In addition, kinetic studies were performed using pseudo-first-order (PFO) and pseudo-second-order (PSO) models. Three experiments were conducted, and the average of the three results was calculated

to minimize errors. We measured the concentrations of MB and CV using a UV-visible spectrophotometer, along with their wavelengths, **Figure S2** and **Figure S3**. We have illustrated the calibration curves for MB and CV Using the Eqs. (1) and (2)[114].

Removal effectiveness and absorption capacity MB and CV were determined every instant[115].

$$\% \text{ Adsorbtion} = \left(\frac{Ci - Ce}{Ci}\right) \times 100 \quad (1)$$

$$Qe = \left(\frac{Ci - Ce}{m}\right) \times V \quad (2)$$

In this relation, Q_e is the absorption capacity ($mg.g^{-1}$), C_i is the initial concentration of the adsorbate in the solution ($L.mg^{-1}$), Ce is the equilibrium concentration of the adsorbate after reaching equilibrium ($L.mg^{-1}$), M is the amount of Ge/Pec-HNTs@IONP magnetic hydrogel halloysite nanotubes (g), and V is the solution.

2.4. Regeneration and reusability

To evaluate the potential for regeneration of the cationic dyes, a retrievability assessment was conducted, Ge/Pec-HNTs@IONP magnetic hydrogel halloysite nanotubes expensive treatment procedures for water treatment. We conducted two consecutive reuse cycles of the Ge/Pec-HNTs@IONP magnetic hydrogel halloysite nanotube regeneration after MB and CV adsorption to evaluate the effectiveness of two consecutive reuse cycles under optimum conditions. The procedure used to conduct the desorption experiment on MB and CV. After MB and CV adsorption by Ge/Pec-HNTs@IONP magnetic hydrogel halloysite nanotubes in optimum conditions, i.e., 10.0 mL of solution volume, 0.003 g of adsorbent dosage, 25 and 20 min contact time duration, solution pH of 8, 150 $mg.L^{-1}$ initial concentration at 25 °C for MB and CV respectively, the magnetic hydrogel halloysite nanotubes the mixture was stirred at 25 °C in a solution of HCl (0.1 M). Desorption was followed by magnetic isolation of the magnetic hydrogel halloysite nanotubes. UV–Vis spectrophotometers determined the amount of released MB and CV. We were using Eqs. (3) we calculated the desorption percentage (D%)[116].

$$D\ (\%) = \frac{A}{B} \times 100 \quad (3)$$

A is the number of impurities adsorbed in the washing solution (mg), and B is the number of contaminants adsorbed on the Ge/Pec-HNTs@IONP magnetic hydrogel halloysite nanotubes (mg).

3. Results and discussion

An organic-inorganic adsorbent synthesized from Ge/Pec hydrogel with abundant amine and carboxyl groups formed by halloysite, which is a hollow tubular structure composed of alumina and silica layers, and the inner surface of the tube has a negative charge, which makes it an ideal material. Ge/Pec-HNTs@IONP magnetic hydrogel halloysite nanotubes were loaded to absorb cationic dyes such as MB and CV. Such magnetization of Ge/Pec-HNTs by IONP resulted in easy recovery of Ge/Pec-HNTs@IONP magnetic hydrogel halloysite nanotubes. Ge/Pec-HNTs@IONP magnetic hydrogel halloysite nanotubes are absorbent. It is active with a porous structure and environmentally friendly properties, essential in removing organic pollutants in its recyclability. Spectral routes will be discussed to investigate the application and performance of the absorber using the captured analyses.

3.1 Characterization

3.1.1. FT-IR spectroscopy

Infrared spectroscopic analysis was used to investigate the preparation of the Ge/Pec-HNTs@IONP magnetic hydrogel halloysite nanotubes and confirm the presence of functional groups, as shown in **Figure 2.** An FT-IR spectrum of HNTs appears in **Figure 2a**. with two distinct peaks at 3696 and 3622 cm^{-1}, corresponding to the surface OH groups within the HNTs lumen and the inner OH groups located between the tetrahedral and octahedral sheets of the HNTs. Besides, the in-plane Si–O–Si stretching mode is detected around 1010 cm^{-1}. In addition, there are bands observed before 1000 cm^{-1} associated with the symmetric stretching modes of the Si–O or Al–O groups. The spectrum of Pec (**Figure 2b**) indicated a peak at 3412.9 cm^{-1} due to the stretching of –OH groups. The peak at 2935.3 and 2927.9 cm^{-1} indicated C–H stretching vibration. The C=O carbonyl stretching vibration describes a strong absorption band

around 1635.5 cm^{-1}. The peaks at 1456 and 1386 cm^{-1} could be assigned to $–CH_2$ scissoring and –OH bending vibration peaks, respectively. The peak at 1045.7 cm^{-1} suggested –CH–O–CH– stretching. The peak at 1132.8 cm^{-1} indicated the presence of–CH–OH in aliphatic cyclic secondary alcohol. According to **Figure 2c**, the absorption peak at 3442.8 cm^{-1} in the FTIR spectrum of Ge can be attributed to N–H stretching and O–H stretching. C–H stretching is responsible for the peak at 29225.4 cm^{-1} and the peak at 2855.7 cm^{-1}. The peak at 1635.5 cm^{-1} represents the absorption band of amide I, while the peak at 1457.5 cm-1 represents the absorption band of amide II. Peaks at 3432 cm^{-1} are due to NH and OH stretching vibration (**Figure 2d**). The absorption peaks at 2930 and 2874 cm^{-1} were assigned to symmetric and asymmetric C-H bonds. The characteristic polysaccharide adsorption bands observed at 1057 cm^{-1} and 1034 cm^{-1} C-O-C glycosidic bond stretches. Also, the peak in the 1420 cm^{-1} and 1628 cm^{-1} region is related to the stretching bond of C-N and C=O of the amide group (type II). The absorption peak observed in 1326 cm^{-1} was attributed to the N-C stretching vibration of amide III and the C=O carbonyl stretching vibration by describing a strong absorption band around 1628 cm^{-1}. Aldimine coupling (AIC) reactions (CH=N) took place during the crosslinking process, and the characteristic absorption of aldimine groups can be seen at 1420 cm^{-1}. Al-OH and Si-O peaks that confirm the presence of HNTs appeared at 3774 cm^{-1} and 900 cm^{-1}. Fe-O absorption band was observed at 674 cm^{-1}, confirming iron nanoparticle synthesis [35].

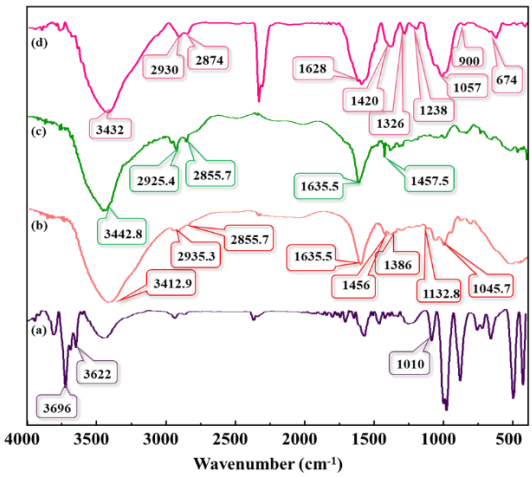

Figure 2. The FT-IR spectra of **(a)** HNTs, **(b)** Pec, **(c)** Ge, and **(d)** Ge/Pec-HNTs@IONP magnetic hydrogel halloysite nanotubes.

3.1.2. XRD analysis

Using an XRD analysis between 5°-70°, the crystallization of the Ge/Pec-HNTs@IONP magnetic hydrogel halloysite nanotubes was evaluated (**Figure 3a**). The XRD analysis of HNTs (**Figure 3a (III)**) corresponding to the JCPDS file No. 29–1487 of HNT showed characteristic peaks at 12.450° and 25.61°, showing a layered structure with SiO_4 tetrahedra and AlO_6 octahedra ordered in an ordered arrangement [117]. The XRD pattern of IONP MNPs (**Figure 3a (II)**) exhibits diffraction, corresponding to the miller indices of the standard formula IONP with card no. JCPDS, 01-074-0748, and the XRD spectra of IONP-MNP reported in the literature ($2\theta = 30.68^{\circ}, 35.90^{\circ}, 43.43^{\circ}, 54.43^{\circ}, 57.46^{\circ}$, and 63.20° The crystal planes in which they are located at (2 2 0), (3 1 1), (4 00), (4 2 2), (3 3 3), and (4 4 0)) [118]. The XRD pattern of the Ge/Pec-HNTs@IONP magnetic hydrogel (incorporating halloysite nanotubes) is displayed. **Figure 3a (I)** presents all the observed diffraction peaks corresponding to the composite material.

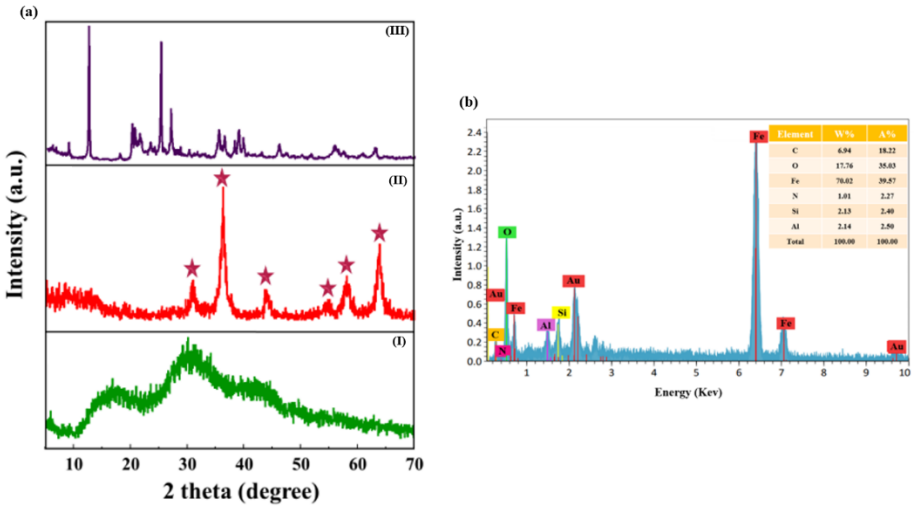

Figure 3. (a) The XRD pattern of (I) Ge/Pec-HNTs@IONP magnetic hydrogel halloysite nanotubes, (II) IONP MNPs, and (III) HNTs, and **(b)** The EDX spectrum of Ge/Pec-HNTs@IONP magnetic hydrogel halloysite nanotubes.

3.1.3. EDX analysis

To identify the elements of the material structure, it was used to identify and confirm the constituent elements of Ge/Pec-HNTs@IONP magnetic hydrogel halloysite nanotubes. As seen in the weight (atomic%), values for carbon (C), oxygen (O), Iron (Fe), nitrogen (N), Silicon (Si), and Al are 6.94% (18.22%), 17.76% (35.03%), 70.02% (39.57), 78.98% (60.87), and 1.01% (2.27%), respectively. The diagram is illustrated in **Figure 3b**. it was confirming the Ge/Pec-HNTs@IONP magnetic hydrogel halloysite nanotubes.

3.1.4. TGA analysis

The thermal stability of Ge/Pec-HNTs@IONP magnetic hydrogel halloysite nanotubes has been investigated using thermal gravimetric analysis in the range of 50 to 800 °C under an N_2 atmosphere (**Figure 4a**). The thermal characteristics behaved in a three-stage breakdown manner between 64 °C and 234 °C, 234 and 450 °C, and 450 and 800 °C. The evaporation of adsorbed water molecules or solvents causes the first step of weight loss (about 3%), which takes place below 200°C. The rapid mass loss lasted from 234 to 450°C, attributed to the dissociation of functional groups and Ge and Pec chains (Step 2). About 78% of this composition's weight has been preserved; the magnetic hydrogel halloysite nanotube bed exhibits high thermal resistance because it contains magnetic iron nanoparticles (Step 3).

3.1.5. VSM analysis

The magnetic properties of Ge/Pec-HNTs@IONP magnetic hydrogel halloysite nanotubes were drawn from -10000 to +10000 Oe, which can be seen in **Figure 4b.** According to the obtained results by comparing IONP (**Figure 4b (I)**) with Ge/Pec-HNTs@IONP magnetic hydrogel halloysite nanotubes (**Figure 4b (II)**) the magnetic saturation of 56.26 $emu.g^{-1}$ and 14.51 $emu.g^{-1}$ are obtained respectively, it can be concluded that there has been a significant reduction, which is due to the non-magnetic property of the Ge/Pec-HNTs.

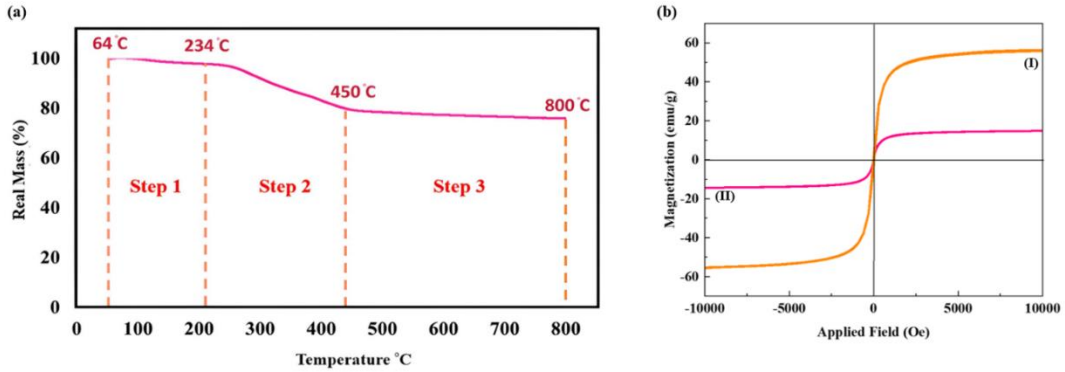

Figure 4. **(a)** TGA curves of Ge/Pec-HNTs@IONP magnetic hydrogel halloysite nanotubes, and **(b)** VSM curves of **(I)** IONP MNPs, and **(II)** Ge/Pec-HNTs@IONP magnetic hydrogel halloysite nanotubes.

3.1.6. FE-SEM analysis

Glutaraldehyde-linked Ge/Pec can be analyzed using SEM (Scanning Electron Microscopy) to understand their structural properties and morphology [119]. The SEM image of glutaraldehyde-linked Ge/Pec hydrogel shows a porous, interconnected network structure with irregularly shaped particles and big pores of glutaraldehyde-linked Ge/Pec hydrogel, most likely as a result of network formation inside the composite hydrogel (**Figure 5a-c**). The surface of the particles appears rough and uneven, indicating the presence of chemical crosslinking between Ge/ Pec hydrogel, which causes a dense network structure, provides mechanical stability, and enhances their functional properties. The Ge/Pec-HNTs@IONP magnetic hydrogel halloysite nanotubes images (**Figure 5d-f**) revealed an irregular texture, and porous cavities on the surface showed relatively large pores.

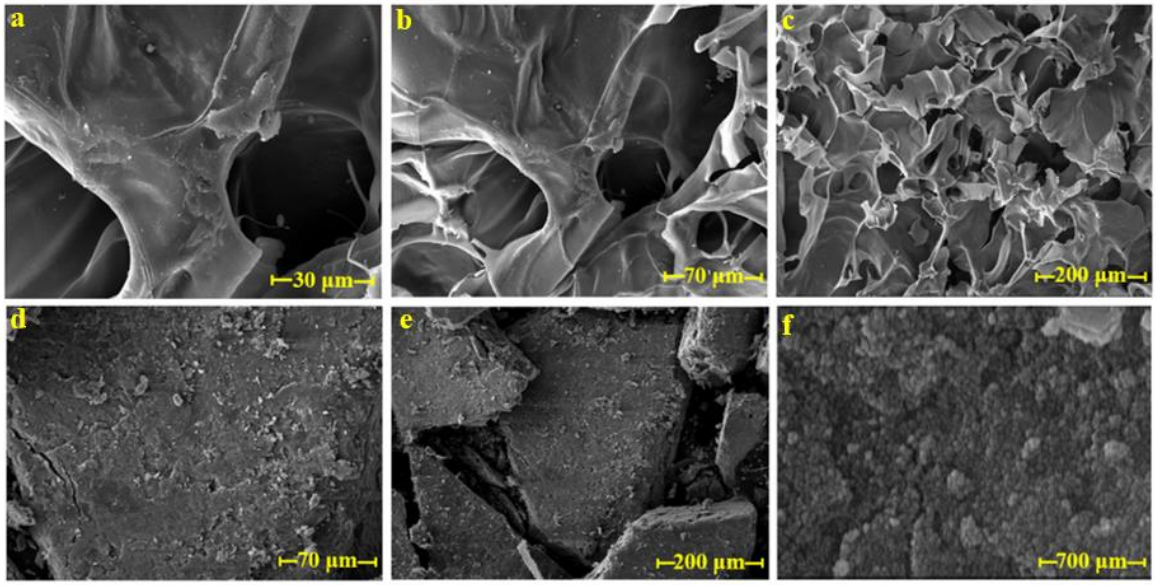

Figure 5. SEM images of **(a-c)** Ge/Pec- HNTs and **(d-f)** Ge/Pec-HNTs@IONP magnetic hydrogel halloysite nanotubes.

3.1.7. BET analysis

The theory of nitrogen gas adsorption and desorption was carried out to understand the physical adsorption of gas molecules on Ge/Pec-HNTs@IONP magnetic hydrogel halloysite nanotubes and Ge/Pec-HNTs as an essential analysis technique for measuring specific surface area, Pore volume, and pore size as illustrated in **Figure 6** [120]. In **Table S3**, BET surface area, pore volume, and average pore diameter of **(a)** Ge/Pec-HNTs and **(b)** Ge/Pec-HNTs@IONP magnetic hydrogel halloysite nanotubes are summarized based on Barrett, Joyner, and Halenda (BJH)

theory. It has been observed in two materials that there is hardly a hysteresis loop in adsorption/desorption isotherms at pressures ranging from 0.45 to 1.0 p/p_0, which indicates that holes are present in mesoporous materials (Type IV). The results of BET are shown in **Table S3**. In the diagram related to the material Ge/Pec-HNTs, the surface area of 7.377 $m^2.g^{-1}$ was measured. After *in-situ* magnetization of IONP, the surface area of Ge/Pec-HNTs@IONP magnetic hydrogel halloysite nanotubes reached 35.244 $m^2.g^{-1}$, and the pore size and pore volume increased. An adsorbent solution for water pollution can be made from microporous magnetic hydrogel halloysite nanotubes with a high porosity structure and a large specific surface area.

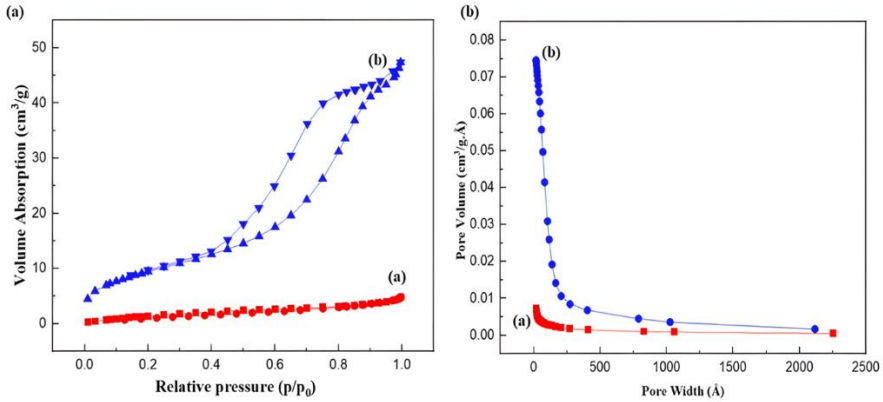

Figure 6. Panel **(a)** is the isotherms of N_2 adsorption-desorption (**a)** Ge/Pec-HNTs, and (**b)** Ge/Pec-HNTs@IONP. Panel **(b)** demonstrates the pore size distribution of **(a)** Ge/Pec-HNTs and **(b)** Ge/Pec-HNTs@IONP magnetic hydrogel halloysite nanotubes.

3.2. Optimization of the effective parameters on the MB and CV adsorption

When using adsorbents, some factors contribute to removing organic contaminants from the water, including the pH, adsorbent dosage, duration time, and concentration of MB and CV in beginning pollutants. Changing these variables can improve the effectiveness of organic pollution removal.

3.2.1. Solution pH

Before optimizing various parameters, calibration curves for the MB and CV dyes are provided in **Figures S1** and **S2**, respectively. Different factors influence the adsorption process of organic dyes, including the pH of the solution, the adsorbent dose used, the contact time, and the initial concentration of the contaminant. Additionally, these parameters can be optimized to improve contaminant removal. The pH effect on the MB and CV adsorption on the Ge/Pec-HNTs@IONP magnetic hydrogel halloysite nanotube is presented in **Figure 7a**. Due to the increased pH of the solution from 4 to 8 for CV and 4 to 10 for MB, the adsorption capacity increased from 138.919 $mg.g^{-1}$ and 89.421 $mg.g^{-1}$ to 148.237 and 132.052 $mg.g^{-1}$, respectively. On the other hand, when the pH was elevated to 10, CV exhibited a reduced adsorption capacity of 141.896, and MB exhibited an increased adsorption capacity of 132.052 $mg.g^{-1}$. Due to the electrostatic repulsion between the OH anions and the OH groups of the magnetic hydrogel halloysite nanotubes, CV has lower adsorption capacities at high pH amounts (i.e., 8). Moreover, both dye molecules with a cationic dye molecule are strongly bonded by hydrogen bonds between Ge/Pec-HNTs@IONP magnetic hydrogel halloysite nanotube. As a result, both dyes operate best at pH 8 and 10 for CV and MB, respectively, which minimizes the amount of cationic and anionic substances located in the solution and assists pollutant and magnetic hydrogel halloysite nanotube interactions. Based on the results of this study, electrostatic attraction was found to be the driving force for MBs and CVs with positively charged structures when the Ge/Pec-HNTs@IONP magnetic hydrogel halloysite nanotube had a negative surface charge, which led to improved adsorption at high pH levels. According to the experimental results, MB and CV had the most excellent adsorption capacity when the solution pH was 10 and 8, respectively.

3.2.2. Adsorbent dosage

Ge/Pec-HNTs@IONP magnetic hydrogel halloysite nanotubes amount at optimum pH=8 for CV and 10 for MB. By **Figure 7b**, as the adsorbent dosage is increased from 0.003 g to 0.03 g, the adsorption capacity of the magnetic hydrogel halloysite nanotubes for MB and CV decreased from ca. 213.947 $mg.g^{-1}$ and 23.807 $mg.g^{-1}$ to 243.018 $mg.g^{-1}$ and 24.8418 $mg.g^{-1}$, respectively. A large amount of MB and CV is available for the adsorption of Ge/Pec-HNTs@IONP magnetic hydrogel halloysite nanotubes. It refers to the increased contaminant amount available to the magnetic hydrogel halloysite nanotubes, resulting in enhanced adsorption capability at lower adsorbent dosages. Therefore, 0.003 g of Ge/Pec-HNTs@IONP magnetic hydrogel halloysite nanotubes, a dose of adsorbent, was most effective for further studies.

3.2.3. Contact time

The effect of contact time of 5, 10, 15, 20, 25, and 30 minutes on pigment capacity in Ge/Pec-HNTs@IONP magnetic hydrogel halloysite nanotubes. At optimum pH=8 and 10 for CV and MB, respectively, 75 $mg.L^{-1}$ of the MB and CV dyes and 0.003 g of adsorbent dose have been studied (**Figure 7c**). The research concluded that the ideal contact times for MB and CV were 25 and 20 minutes, respectively. Initial interactions between dye molecules in an aqueous solution and many vacant magnetic hydrogel halloysite nanotube sites allow for a rapid mass transfer. The interactions between adsorbent functional groups and MB and CV become more intense as contact time is extended to 25 min (215.289 $mg.g^{-1}$) and 20 min (249.189 $mg.g^{-1}$) until the maximum equilibrium adsorption capacity is reached. After this point, however, there was no further improvement in adsorption capacity, which can be attributed to the Ge/Pec-HNTs@IONP magnetic hydrogel halloysite nanotubes approaching equilibrium and occupying active sites.

3.2.4. The initial concentration

It is generally agreed that the initial concentration of the cationic dye is one of the most critical and influential variables involved in the adsorption process. The effect of the initial concentration of MB and CV on the effectiveness of its removal by Ge/Pec-HNTs@IONP magnetic hydrogel halloysite nanotubes was studied. The initial concentrations of the dye studied were 25, 50, 75, 100, 125 and 150 $mg.L^{-1}$. The conditions studied were optimal (pH=10 and 8, Time 25 and 20 minutes for MB and CV, respectively, and adsorbent dosage 0.003 g). The effect of the initial concentration of MB and CV on adsorption capacity by the synthesized adsorbent is depicted in **Figure 7d**. It is evident that lowering the starting concentration of cationic dye from 25 $mg.L^{-1}$ to 150 $mg.L^{-1}$ reduces the adsorption capacity of 79.298 to 582.22 and 82.689 to 485.535 for MB and CV, respectively. The saturation of the adsorbent surface at high cationic dye concentrations was the primary factor responsible for this declining trend. The number of active sites on the adsorbent remained constant despite a rise in the overall number of cationic dye molecules, which caused this event. As a result, the findings above suggest that the adsorption processes at high concentrations of the adsorbed material depend on the concentration at the beginning of the experiment. It also shows that increasing the dye's initial concentration positively affects the adsorption capacity. Additionally, the maximum adsorption percentages for the cationic dyes MB and CV by the Ge/Pec-HNTs@IONP magnetic hydrogel halloysite nanotubes adsorbent are 76.91% and 97.10%, respectively.

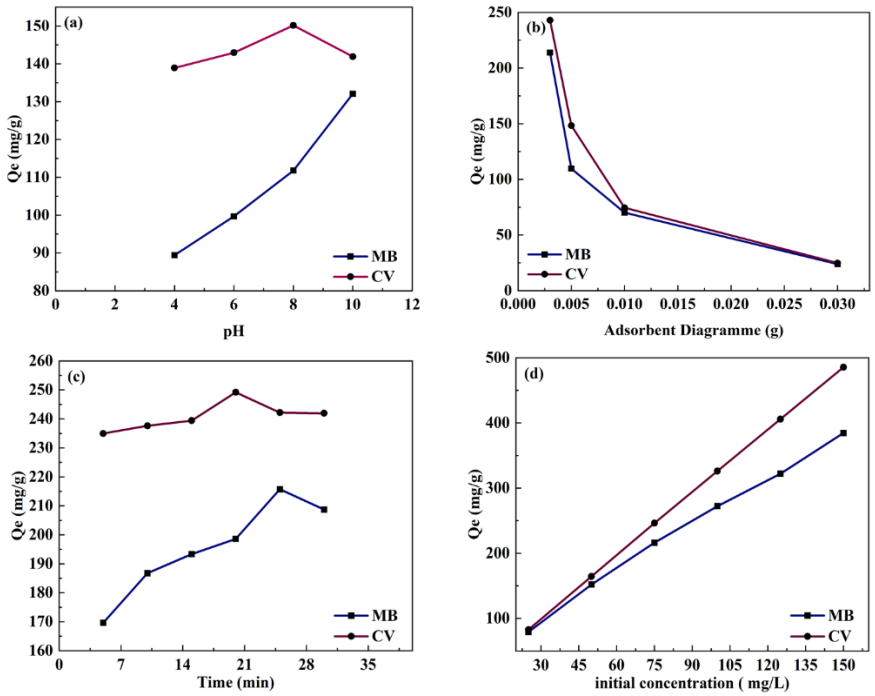

Figure 7. (a) solution affects pH (4- 10), **(b)** adsorbent dosage (0.003- 0.03 g), **(c)** contact time (5–30 min), and **(d)** initial concentration (50–400 mg.L^{-1}).

3.3. Adsorption isotherm and kinetics studies

In the present work, MB and CV interact with organic pollution via the adsorption isotherm investigation of Ge/Pec-HNTs@IONP magnetic hydrogel halloysite nanotubes. Langmuir and Freundlich's models have analyzed adsorption equilibrium isotherms and maximum adsorption capacity. The Langmuir isotherm explains how organic contamination adsorbs into a single layer of adsorbents. During homogeneous adsorption, all sites in the adsorbent interact with the contaminant regardless of their energy, affinity, or surface area. The organic contamination forms a complete monolayer on the surface of the adsorbent to achieve maximum adsorption capacity. A multilayer adsorption model based on heterogeneous surfaces of adsorbents, unlike Freundlich's model. An adsorbent's heterogeneous surface allows multilayer adsorption of contaminants. These formulas correspond to the Langmuir Eqs (4) and Freundlich (5) models[121].

$$\frac{C_e}{q_e} = \frac{1}{K_L Q_{max}} + \frac{1}{Q_{max}} C_e \quad (4)$$

$$ln\, q_e = ln\, K_F \; + \frac{1}{n} ln\, C_e\, ln\, q_e \quad (5)$$

The Q_e and Q_{max} represent the equilibrium MB and CV concentrations (mg.L^{-1}), C_e is the equilibrium MB and CV concentration (mg.L^{-1}), and K_L (L.mg^{-1}) is the equilibrium adsorption capacity. According to C_e/Q_e plots and Ce lnQ_e plots. MB and CV can be absorbed in high concentrations from the adsorbent when n > 1. **Figure 8a** and **b**. shows the Langmuir and Freundlich isotherm charts; details of both isotherms are illustrated in **Table S4**. MB and CV are better suited to the Freundlich isotherm than the Langmuir isotherm. Compared to other adsorbents, it has shown the most excellent adsorption capacity for the MB and CV. The fabricated nanocomposites exhibited excellent Q_{max} compared to various other adsorbents previously reported. Several physicochemical characteristics associated with fabricated adsorbent systems contribute to the high values of Q_{max}, including easy diffusion of organic pollutants into Ge/Pec-HNTs@IONP magnetic hydrogel halloysite nanotubes. These magnetic hydrogel halloysite nanotubes effectively remove cationic dyes from wastewater contamination by absorbing them. The study and forecasting of different adsorption processes, equilibrium times, and the rate-limiting stage of the adsorption process can all be done using adsorption kinetics. Based on pseudo-first-order (PFO) and pseudo-second-order (PSO) models, this study

investigated the MB and CV adsorption rates onto the Ge-Pec hydrogel-HNTs/IONP magnetic hydrogel halloysite nanotubes adsorbent. They are mathematically expressed using Eqs. (6) and (7), respectively[121].

$$\mathrm{Log}(Q_e - Q_t) = \mathrm{Log}Q_e - \frac{k_1}{2.303}t \quad (6)$$

$$\frac{t}{Q_t} = \frac{1}{k_2 Q_e^2} + \frac{1}{Q_e}t \quad (7)$$

Here, Q_t stands for the period adsorption capacity of the Ge/Pec-HNTs@IONP magnetic hydrogel halloysite nanotubes, and Q_e (mg.g^{-1}) for the Hassan equilibrium adsorption capacity. The PSO rate constant is K_2 (g.mg.min^{-1}) according to the PFO rate constant K_1(1/min). In **Figure 8c** and **d** and **Table S4**. With the pertinent data, the linear kinetic graphs are displayed. MB and CV adsorption kinetics on Ge/Pec-HNTs@IONP magnetic hydrogel halloysite nanotubes is better explained by the PSO model, according to correlation coefficients and differences between calculated and observed Q_e values of the two kinetic models under investigation.

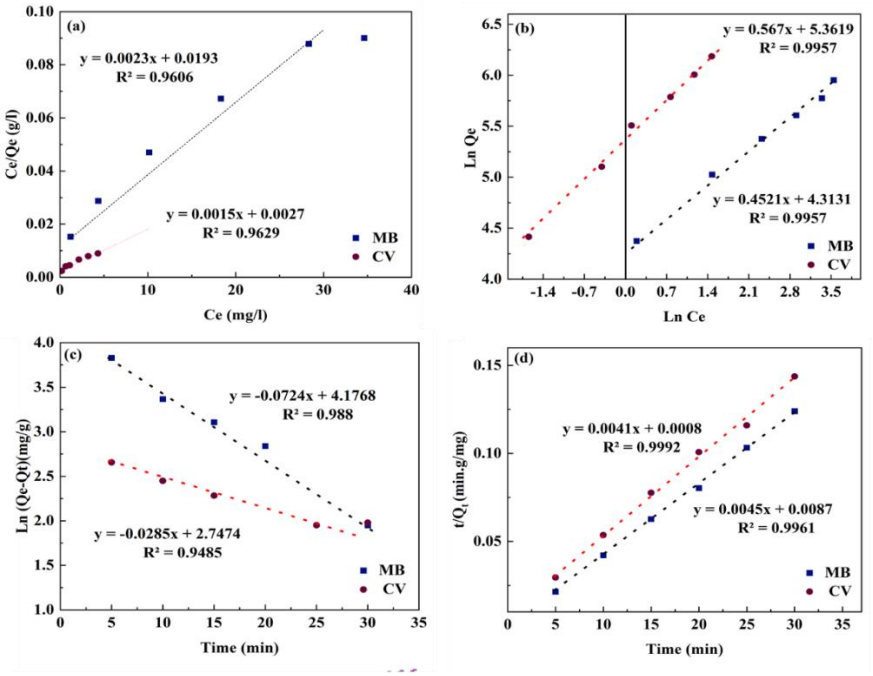

Figure 8. (a) Langmuir, **(b)** Freundlich isotherms, **(c)** pseudo-first-order (PFO), and **(d)** pseudo-second-order (PSO) models.

Table 1. Compared to earlier published investigations, an assessment of the material's maximum adsorption capacity Ge/Pec-HNTs@IONP magnetic hydrogel halloysite nanotubes.

Adsorbent	Q_{max} (mg.g^{-1}) MB	Ref.	Adsorbent	Q_{max} (mg.g^{-1}) CV	Ref.
Xylan and gelatin	26.04	[122]	Pect/AILP-Kal nanocomposite	72	[123]
Pectin membrane	19.39	[124]	Mag./silica/pectin NPs	125	[125]
(Pect/AILP-Kal) nanocomposite	76	[123]	Gelatin hydrogel (GH)	138.89 [1]	[125]
GT-CAG-cl-polyAA	94.9	[126]	Gelatin/Chitosan hydrogel	233.4	[127]
PAC-nZVI	99	[128]	Pec-g-poy (AMPS-co-AAm)	329	[129]
Dop-Pec hydrogel	111.1	[130]	PAC-nZVI	344	[128]
Ge/Pec	123.54	Present work	Ge/Pec	156.76	Present work
Ge/Pec-HNTs@IONP	384.561	Present work	Ge/Pec-HNTs@IONP	485.534	Preset work

3.4. Recovery and reusability

The reusability of Ge/Pec-HNTs@IONP magnetic hydrogel halloysite nanotubes was examined to research the absorption of MB and CV dyes. Three sequential adsorption and desorption cycles were carried out to test the recyclability of Ge/Pec-HNTs@IONP magnetic hydrogel halloysite nanotubes, according to the results shown in **Figure S4.** Reusing adsorbents can save money and energy, which is why, after MB and CV were adsorbed on the Ge/Pec-HNTs@IONP magnetic hydrogel halloysite nanotubes, the desorption process was carried out by soaking the material in an HCl solution of 0.1 M at ambient temperature. After being removed from a magnet, the adsorbent was repeatedly cleaned in d.w. and ethanol. The adsorption percentages after two cycles change from 76.91 to 65.070% and 97.107% to 94.45%, and the desorption percentages change from 84.23% to 80.82% and 82.42% to 79.32% for MB and CV, respectively. The results demonstrate that the magnetic hydrogel halloysite nanotubes can desorb and resorb MB and CV for two more cycles without significantly reducing adsorption capacity.

3.5. Suggested mechanisms for the adsorption process

There are several phases in the adsorption mechanism of Ge/Pec-HNTs@IONP magnetic hydrogel halloysite nanotubes to remove MB and CV dyes (**Figure 9**). The hydrogel matrix, in the first place, provides a porous structure that enables MB and CV dyes to penetrate the hydrogel. HNTs present in the hydrogel increase the ability of the hydrogel to absorb materials due to their high surface area and abundant OH groups on the surface and inside by creating hydrogen bonds with MB and CV dyes. Also, functional groups in MB and CV structures participate in electrostatic interactions with functional groups on surfaces. In addition, the Ge/Pec hydrogel has functional groups, such as amino groups, that can form hydrogen bonds with MB and CV dyes through van der Waals forces. A very effective adsorbent for removing MB and CV dyes from aqueous solutions is created by Ge/Pec-HNTs@IONP magnetic hydrogel halloysite nanotubes.

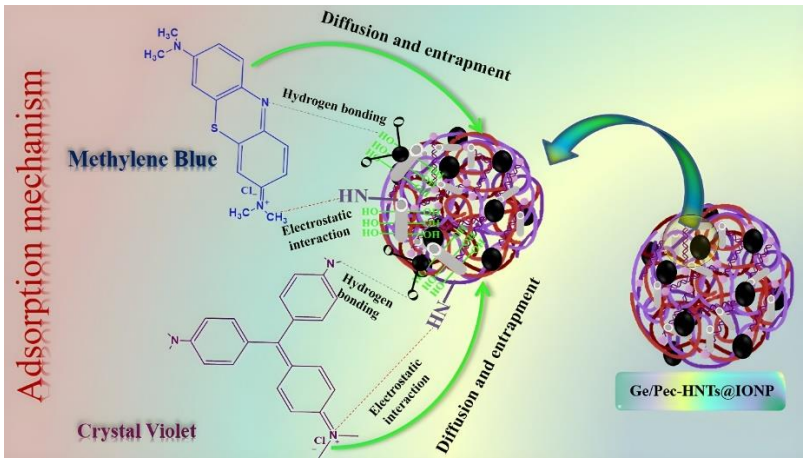

Figure 9. The suggested mechanism for adsorption of MB and CV by the Ge/Pec-HNTs@IONP magnetic hydrogel halloysite nanotubes.

4. Conclusions

Using HNTs, Ge/Pec hydrogel, and IONP MNPs, a practical, cost-effective, and environmentally friendly adsorbent Ge/Pec-HNTs@IONP magnetic hydrogel halloysite nanotubes was created in this study to treat wastewater containing dangerous organic compounds including MB and CV-dyes. Ge/Pec-HNTs@IONP magnetic hydrogel halloysite nanotubes have a considerable elimination percentage of 87.33% and 86.69% for MB and CV dyes, respectively, according to the data obtained under ideal conditions. The Freundlich model was used to interpret these experimental findings on the adsorption of the dye's CV and MB on the Ge/Pec-HNTs@IONP magnetic hydrogel halloysite nanotubes, with maximal adsorption capacities of 582.21 and 577.95 $mg.g^{-1}$ for CV and MB, respectively. The model with the best fit to the experimental data was PSO model kinetics. The experiment's outcomes suggest that chemical processes impact the dye's CV and MB adsorption. Finally, this research demonstrates that the created Ge/Pec-

HNTs@IONP magnetic hydrogel halloysite nanotubes are an effective adsorbent composite for wastewater treatment and cationic dye pollution removal.

Authors' contributions

Leila Choopani: Contributed to the conception, design, and drafting of the work, preparing figures, reviewing them, leading adsorption experiments, and editing. **Mohammad Mehdi Salehi:** Preparing Figures, reviewing, and editing. **Reza Eivazzadeh-Keihan:** The corresponding author of the current study, who made substantial contributions to the conception, design, drafting, writing, reviewing, and editing of the work and substantively revised it. **Ali Maleki:** The corresponding author of the current study, who made substantial contributions to the conception, design, drafting, writing, reviewing, and editing of the work and substantively revised it.

Declaration of competing interest

The authors declare that they have no known competing financial interests or personal relationships that could have appeared to influence the work reported in this paper.

Funding

This paper received no funding.

Acknowledgment

The authors gratefully acknowledge the partial support from the Research Council of the Iran University of Science and Technology (IUST).

Data availability

Data will be made available on request.

References

[1] G. Wood, C. Bischoff, Challenges and progress in integrating knowledge: cases from clothing and textiles in South Africa, J. Knowl. Manag. 24 (2020) 32–55.
DOI: https://doi.org/10.1108/JKM-04-2019-0168
[2] E. Moradi, M.M. Salehi, A. Maleki, Highly stable mesoporous Co/Ni mixed metal-organic framework [Co/Ni (μ3-tp) 2 (μ2-pyz) 2] for Co(II) heavy metal ions (HMIs) remediation, Heliyon 10 (2024) e37502.
DOI: https://doi.org/10.1016/j.heliyon.2024.e37502
[3] K. Saha, P.K. Dey, E. Papagiannaki, Implementing circular economy in the textile and clothing industry, in: Supply Chain Sustainability in Small and Medium Sized Enterprises, Routledge, 2022, pp. 239–276.
DOI: https://doi.org/10.4324/9781003178034
[4] P. Beigi, F. Ganjali, F. Hassanzadeh-Afruzi, M.M. Salehi, A. Maleki, Enhancement of adsorption efficiency of crystal violet and chlorpyrifos onto pectin hydrogel@Fe3O4-bentonite as a versatile nanoadsorbent, Sci. Rep. 13 (2023) 10764.
DOI: https://doi.org/10.1038/s41598-023-37874-8
[5] S. Nicolai, T. Tralau, A. Luch, R. Pirow, A scientific review of colorful textiles, J. Consum. Prot. Food Saf. 16 (2021) 5–17. DOI: https://doi.org/10.1007/s00003-020-01281-2
[6] J. Govey-Scotland, L. Johnstone, C. Myant, M.S. Friddin, Towards skin-on-a-chip for screening the dermal absorption of cosmetics, Lab Chip 23 (2023) 746–767.
DOI: https://doi.org/10.1039/D2LC00799E
[7] T. Kaseke, T. Lujic, T.C. Velickovic, Nano- and microplastics migration from plastic food packaging into dairy products: impact on nutrient digestion, absorption, and metabolism, Foods 12 (2023) 3043.
DOI: https://doi.org/10.3390/foods12163043
[8] E. Reale, D. Vernez, N.B. Hopf, Skin absorption of bisphenol A and its alternatives in thermal paper, Ann. Work Expo. Health 65 (2021) 206–218.
DOI: https://doi.org/10.1093/annweh/wxaa088
[9] S. Pratheba, N. Balasundaram, P. Preethi, Isolated microbial decolorization of textile dye effluent, Mater. Today: Proc. 72 (2023) 3133–3136.
DOI: https://doi.org/10.1016/j.matpr.2022.08.167
[10] C.F. Carolin, P.S. Kumar, G.J. Joshiba, Sustainable approach to decolourize methyl orange dye from aqueous solution using novel bacterial strain and its metabolites characterization, Clean Technol. Environ. Policy 23 (2021) 173–181.
DOI: https://doi.org/10.1007/s10098-020-01967-z

[11] R.J. Nascimento, K.R.A. Pereira, F. Avelino, Parametric and modeling studies of Rhodamine-B adsorption using coconut coir-based materials as eco-friendly adsorbents, J. Environ. Chem. Eng. 9 (2021) 105943.
DOI: https://doi.org/10.1016/j.jece.2021.105943
[12] B. Wang, T. Wang, H. Su, A dye-methylene blue (MB)-degraded by hydrodynamic cavitation (HC) and combined with other oxidants, J. Environ. Chem. Eng. 10 (2022) 107877.
DOI: https://doi.org/10.1016/j.jece.2022.107877
[13] L. Choopani, M. Heydari, F. Ganjali, A. Maleki, Removal of organic contamination from wastewater using granular activated carbon modified—polyethylene glycol: characterization, kinetics and isotherm study, PLoS ONE 19 (2024) e0304684.
DOI: https://doi.org/10.1371/journal.pone.0304684
[14] P.O. Oladoye, M.O. Bamigboye, O.D. Ogunbiyi, M.T. Akano, Toxicity and decontamination strategies of Congo red dye, Groundw. Sustain. Dev. 19 (2022) 100844.
DOI: https://doi.org/10.1016/j.gsd.2022.100844
[15] H.S. Al-Shehri, E. Almudaifer, A.Q. Alorabi, H.S. Alanazi, A.S. Alkorbi, F.A. Alharthi, Effective adsorption of crystal violet from aqueous solutions with effective adsorbent: equilibrium, mechanism studies and modeling analysis, Environ. Pollut. Bioavailab. 33 (2021) 214–226.
DOI: https://doi.org/10.1080/26395940.2021.1960199
[16] F. Hassanzadeh-Afruzi, G. Ranjbar, M.M. Salehi, F. Esmailzadeh, A. Maleki, Thiacalix[4]arene-functionalized magnetic xanthan gum (TC4As-XG@Fe3O4) as a hydrogel adsorbent for removal of dye and pesticide from water medium, Sep. Purif. Technol. 306 (2023) 122700.
DOI: https://doi.org/10.1016/j.seppur.2022.122700
[17] M.S.J. Zadegan, M. Arjmand, M.M. Salehi, F. Ganjali, A. Maleki, Remediation of safranin-O and acid fuchsin by using Ti3C2 MXene/rGO-Cu2O nanocomposite: preparation, characterization, isotherm, kinetic and thermodynamic studies, Environ. Res. 258 (2024) 119469.
DOI: https://doi.org/10.1016/j.envres.2024.119469
[18] R. Santos, É.F. Silva, E.J. Dantas, E.D. Oliveira, T.B. Simões, Í.R. Araújo, A.T. Ribeiro, L.P. Oliveira, R.R. Garcia, L.C. Almeida, Potential reuse of PET waste bottles as a green substrate/adsorbent for reactive black 5 dye removal, Water Air Soil Pollut. 231 (2020) 1–16.
DOI: https://doi.org/10.1007/s11270-020-04878-3
[19] M. Wang, C. Guo, C. Li, T. Zhao, Design of novel reactive dyes containing cationic groups: mechanism and application for environmentally friendly cotton dyeing, Fibers Polym. 21 (2020) 2848–2860.
DOI: https://doi.org/10.1007/s12221-020-1035-x
[20] I. Khan, K. Saeed, I. Zekker, B. Zhang, A.H. Hendi, A. Ahmad, S. Ahmad, Review on methylene blue: its properties, uses, toxicity and photodegradation, Water 14 (2022) 242.
DOI: https://doi.org/10.3390/w14020242
[21] S. Sarkar, S.S. Gill, G.D. Gupta, S.K. Verma, Water toxicants: a comprehension on their health concerns, detection, and remediation, Environ. Sci. Pollut. Res. 29 (2022) 53934–53953.
DOI: https://doi.org/10.1007/s11356-022-21037-9
[22] S.N. Taqui, M. Cs, M.S. Goodarzi, M.A. Elkotb, B.A. Khatoon, M.E.M. Soudagar, I.B. Koki, A. Elfasakhany, A.S. Khalifa, M.A. Ali, Sustainable adsorption method for the remediation of crystal violet dye using nutraceutical industrial fenugreek seed spent, Appl. Sci. 11 (2021) 7635.
DOI: https://doi.org/10.3390/app11167635
[23] H. Bian, S. Duan, J. Wu, Y. Fu, W. Yang, S. Yao, Z. Zhang, H. Xiao, H. Dai, C. Hu, Lignocellulosic nanofibril aerogel via gas phase coagulation and diisocyanate modification for solvent absorption, Carbohydr. Polym. 278 (2022) 119011.
DOI: https://doi.org/10.1016/j.carbpol.2021.119011
[24] A.M. Horstman, T. Huppertz, Milk proteins: processing, gastric coagulation, amino acid availability and muscle protein synthesis, Crit. Rev. Food Sci. Nutr. 63 (2023) 10267–10282.
DOI: https://doi.org/10.1080/10408398.2022.2078782
[25] N. Sedaghati, A. Habibi-Yangjeh, S. Asadzadeh-Khaneghah, S. Ghosh, Photocatalytic performance of oxygen vacancy rich-TiO2 combined with Bi4O5Br2 nanoparticles on degradation of several water pollutants, Adv. Powder Technol. 32 (2021) 304–316.
DOI: https://doi.org/10.1016/j.apt.2020.12.013
[26] C. Li, L. He, X. Yao, Z. Yao, Recent advances in the chemical oxidation of gaseous volatile organic compounds (VOCs) in liquid phase, Chemosphere 295 (2022) 133868.
DOI: https://doi.org/10.1016/j.chemosphere.2022.133868
[27] Y. Liao, G. He, Y. Duan, Morphology-controlled self-assembly synthesis and excellent microwave absorption performance of MnO_2 microspheres of fibrous flocculation, Chem. Eng. J. 425 (2021) 130512.
DOI: https://doi.org/10.1016/j.cej.2021.130512
[28] F. Shi, J. Gu, D. Ying, K. Li, N. Yan, J. Li, J. Jia, Absorption and recovery of SO2 in flue gas by wet absorption combined with bipolar membrane electrodialysis, Chem. Eng. J. 433 (2022) 134595.
DOI: https://doi.org/10.1016/j.cej.2021.134595
[29] P. Alfonso-Muniozguren, E.A. Serna-Galvis, M. Bussemaker, R.A. Torres-Palma, J. Lee, A review on pharmaceuticals removal from waters by single and combined biological, membrane filtration and ultrasound systems, Ultrason. Sonochem. 76

(2021) 105656.
DOI: https://doi.org/10.1016/j.ultsonch.2021.105656
[30] F. Hassanzadeh-Afruzi, F. Esmailzadeh, S. Asgharnasl, F. Ganjali, R. Taheri-Ledari, A. Maleki, Efficient removal of Pb(II)/Cu(II) from aqueous samples by a guanidine-functionalized SBA-15/Fe3O4, Sep. Purif. Technol. 291 (2022) 120956.
DOI: https://doi.org/10.1016/j.seppur.2022.120956
[31] C. Nam, Y. Lee, H. Lee, Y. Lee, Y. Lee, K. Kim, Increased hydrogel swelling induced by absorption of small molecules, ACS Appl. Mater. Interfaces 8 (2016) 14263–14270.
DOI: https://doi.org/10.1021/acsami.6b03269
[32] D. Joshy, N.K. Puthenveettil, Y.A. Ismail, P. Periyat, Mechanistic investigation of mesoporous Mg2+ doped CeO2 encapsulated Fe3O4 core-shells for the selective adsorptive removal of malachite green, Results Eng. 20 (2023) 101409.
DOI: https://doi.org/10.1016/j.rineng.2023.101409
[33] A. Banerjee, T. Bhaskar, D. Ghosh, A biorefinery approach for sewage sludge, in: Waste Biorefinery, Elsevier, 2020, 393–421.
DOI: https://doi.org/10.1016/B978-0-12-818228-4.00014-4
[34] M. Salehi, F. Hassanzadeh Afruzi, F. Esmailzadeh, L. Choopani, K. Rajabi, H. Kuzekanan, M. Azizi, F. Yeganeh, O. Demchuk, A. Maleki, Chlorpyrifos and diazinon elimination through pAAm-g-XG/HKUST-1@Fe3O4 biopolymer nanoadsorbent hydrogel from wastewater: preparation, characterization, kinetics and isotherm, Sep. Purif. Technol. 334 (2023) 126097.
DOI: https://doi.org/10.1016/j.seppur.2023.126097
[35] R. Eivazzadeh-Keihan, L. Choopani, H.A.M. Aliabadi, F. Ganjali, A. Kashtiaray, A. Maleki, R.A. Cohan, M.S. Bani, S. Komijani, M.M. Ahadian, N. Salehpour, M. Mahdavi, Magnetic carboxymethyl cellulose/silk fibroin hydrogel embedded with halloysite nanotubes as a biocompatible nanobiocomposite with hyperthermia application, Mater. Chem. Phys. 287 (2022) 126347.
DOI: https://doi.org/10.1016/j.matchemphys.2022.126347
[36] M.M. Salehi, F. Hassanzadeh-Afruzi, G. Heidari, A. Maleki, E.N. Zare, In situ preparation of MOF-199 into the carrageenan-grafted-polyacrylamide@Fe3O4 matrix for enhanced adsorption of levofloxacin and cefixime antibiotics from water, Environ. Res. 233 (2023) 116466.
DOI: https://doi.org/10.1016/j.envres.2023.116466
[37] M.J. Sharifi, A. Nouralishahi, A. Hallajisani, Fe3O4-chitosan nanocomposite as a magnetic biosorbent for removal of nickel and cobalt heavy metals from polluted water, Int. J. Biol. Macromol. 248 (2023) 125984.
DOI: https://doi.org/10.1016/j.ijbiomac.2023.125984
[38] X. Chen, H. Liu, D. Hu, H. Liu, W. Ma, Recent advances in carbon nanotubes-based microwave absorbing composites, Ceram. Int. 47 (2021) 23749–23761.
DOI: https://doi.org/10.1016/j.ceramint.2021.05.095
[39] T. Guo, X. Wang, J. Guo, C. Zhang, Recent progress in MOF-aerogel fabrication and applications, Small (2024) 2402942.
DOI: https://doi.org/10.1002/smll.202402942
[40] F. Hassanzadeh-Afruzi, M. Forouzandeh-Malati, F. Ganjali, M.M. Salehi, A. Maleki, E.N. Zare, Carrageenan-grafted-poly(acrylamide) magnetic nanocomposite modified with graphene oxide for ciprofloxacin removal from polluted water, Alex. Eng. J. 82 (2023) 503–517.
DOI: https://doi.org/10.1016/j.aej.2023.09.066
[41] L. Choopani, H.A.M. Aliabadi, F. Ganjali, A. Kashtiaray, R. Eivazzadeh-Keihan, A. Maleki, M. Mahdavi, Functionalization of zinc ferrites nanoparticles by cyclic aromatic polyimide chains as a novel star polymer with antibacterial activity and low toxicity, J. Ind. Eng. Chem. (2024).
DOI: https://doi.org/10.1016/j.jiec.2024.01.047
[42] Z. Hajizadeh, M.M. Salehi, MOFs bandstructure, in: Physicochemical Aspects of Metal-Organic Frameworks: A New Class of Coordinative Materials, Springer, 2023, pp. 79–90.
DOI: https://doi.org/10.1007/978-3-031-18675-2_5
[43] M.M. Salehi, F. Hassanzadeh Afruzi, F. Esmailzadeh, L. Choopani, K. Rajabi, H. Kuzekanan, M. Azizi, F. Yeganeh, O. Demchuk, A. Maleki, Chlorpyrifos and diazinon elimination through pAAm-g-XG/HKUST-1@Fe3O4 biopolymer nanoadsorbent hydrogel from wastewater: preparation, characterization, kinetics and isotherm, Sep. Purif. Technol. 334 (2023) 126097.
DOI: https://doi.org/10.1016/j.seppur.2023.126097
[44] D. Gul, S. Khan, S. Muhammad, T. Kamal, Contamination by hazardous elements in low-priced children's plastic toys bought on the local markets of Karachi, Pakistan, Environ. Sci. Pollut. Res. 29 (2022) 51964–51975.
DOI: https://doi.org/10.1007/s11356-022-19425-2
[45] M. Dohendou, M.G. Dekamin, D. Namaki, Supramolecular Pd@methionine-EDTA-chitosan nanocomposite: an effective and recyclable bio-based and eco-friendly catalyst for the green Heck cross-coupling reaction under mild conditions, Nanoscale Adv. 5 (2023) 2621–2638.
DOI: https://doi.org/10.1039/D2NA00933B
[46] I. Zare, M. Tavakol, M. Montazer, M. Rezayat, S.M. Naghib, DNA hydrogels and nanogels for diagnostics, therapeutics, and theragnostic of various cancers, Nanoscale 15 (2023) 11325–11353.
DOI: https://doi.org/10.1039/D3NR01250H

[47] M.M. Salehi, F. Esmailzadeh, F. Hassanzadeh-Afruzi, Applications of MOFs, in: Physicochemical Aspects of Metal-Organic Frameworks: A New Class of Coordinative Materials, Springer, 2023, pp. 197–305.
DOI: https://doi.org/10.1007/978-3-031-18675-2_7
[48] A.M. Elgarahy, K.Z. Elwakeel, G.A. Elshoubaky, S.H. Mohammad, A critical review of biosorption of dyes, heavy metals and metalloids from wastewater as an efficient and green process, Clean. Eng. Technol. 4 (2021) 100209.
DOI: https://doi.org/10.1016/j.clet.2021.100209
[49] R. Eivazzadeh-Keihan, H.A.M. Aliabadi, L. Choopani, M.G. Gorab, S. Rahmati, A. Kashtiaray, M. Mahdavi, A. Maleki, Functionalization of chitosan by metformin, nickel metal ions and magnetic nanoparticles as a nanobiocomposite for purification of alkaline phosphatase from hen's egg yolk, J. Chromatogr. A 1679 (2022) 463376.
DOI: https://doi.org/10.1016/j.chroma.2022.463376
[50] M. Yang, Y. Yuan, Y. Li, X. Sun, S. Wang, L. Liang, Y. Ning, J. Li, Y. Yin, R. Che, Anisotropic electromagnetic absorption of aligned Ti3C2Tx MXene/gelatin nanocomposite aerogels, ACS Appl. Mater. Interfaces 12 (2020) 33128–33138.
DOI: https://doi.org/10.1021/acsami.0c09798
[51] M. Dohendou, M.G. Dekamin, D. Namaki, Pd@l-asparagine–EDTA–chitosan: a highly effective and reusable bio-based and biodegradable catalyst for the Heck cross-coupling reaction under mild conditions, Nanoscale Adv. 5 (2023) 2621–2638.
DOI: https://doi.org/10.1039/D2NA00933B
[52] Y. Zhang, M. Lin, Y. Zhang, J. Xiao, Y. Sui, Q. Wang, L. Zhang, Oral absorption characteristics and mechanisms of a pectin-type polysaccharide from Smilax china L. across the intestinal epithelium, Carbohydr. Polym. 270 (2021) 118383.
DOI: https://doi.org/10.1016/j.carbpol.2021.118383
[53] F. Hassanzadeh-Afruzi, M.M. Salehi, F. Ganjali, M. Heydari, A. Maleki, Facile synthesis of pyrazolopyridine pharmaceuticals under mild conditions using an algin-functionalized silica-based magnetic nanocatalyst (Alg@SBA-15/Fe3O4), RSC Adv. 13 (2023) 10367–10378.
DOI: https://doi.org/10.1039/D3RA01337G
[54] M.M. Salehi, F. Hassanzadeh-Afruzi, G. Heidari, A. Maleki, Performance of magnetic nanocomposite based on xanthan gum-grafted-poly(acrylamide) crosslinked borax for the effective elimination of amoxicillin from an aquatic environment, Chemosphere (2024) 142548.
DOI: https://doi.org/10.1016/j.chemosphere.2024.142548
[55] S.B. Khan, M.A. Bakhsh, F. Akhtar, S. Ali, S. Almojil, A. Almohamadi, 3D printed nanofiltration membrane technology for waste water distillation, J. Water Process Eng. 49 (2022) 102958.
DOI: https://doi.org/10.1016/j.jwpe.2022.102958
[56] M. Mele, M. Ricciarelli, G. Campana, 3D printing of clay paste enhanced by scrap polymer from powder bed processes, Rapid Prototyp. J. 28 (2022) 285–296.
DOI: https://doi.org/10.1108/RPJ-10-2020-0248
[57] C. Zhang, W. Zhang, Z. Ji, X. Wang, S. Li, S. Wang, Three-dimensional electrochemical sensors for food safety applications, Biosensors 13 (2023) 529.
DOI: https://doi.org/10.3390/bios13050529
[58] M.M.A. Arif, M.B. Fauzi, A. Nordin, Y. Hiraoka, Y. Tabata, M.H.M. Yunus, Fabrication of bio-based gelatin sponge for potential use as a functional acellular skin substitute, Polymers 12 (2020) 2678.
DOI: https://doi.org/10.3390/polym12112678
[59] X. Ding, X. Cai, J. Bian, Y. Liu, Q. Wang, D. Liu, Gelatin as green adhesive for the preparation of a multifunctional biobased cryogel derived from bamboo industrial waste, Carbohydr. Polym. 255 (2021) 117340.
DOI: https://doi.org/10.1016/j.carbpol.2020.117340
[60] F. Mushtaq, A. Raza, N. Ghauri, M. Zafar, M. Agib, Z. Ilyas, M. Ikram, Preparation, properties, and applications of gelatin-based hydrogels (GHs) in the environmental, technological, and biomedical sectors, Int. J. Biol. Macromol. 218 (2022) 601–633.
DOI: https://doi.org/10.1016/j.ijbiomac.2022.07.168
[61] I. Lukin, D. Erezuma, T. Desimone, G. Orive, Progress in gelatin as biomaterial for tissue engineering, Pharmaceutics 14 (2022) 1177.
DOI: https://doi.org/10.3390/pharmaceutics14061177
[62] N.S. Said, N.K. Howell, N.M. Sarbon, A review on potential use of gelatin-based film as active and smart biodegradable films for food packaging application, Food Rev. Int. 39 (2023) 1063–1085.
DOI: https://doi.org/10.1080/87559129.2021.1934002
[63] B. Salahuddin, S. Wang, M. Sangian, S. Aziz, G. Gu, Hybrid gelatin hydrogels in nanomedicine applications, ACS Appl. Bio Mater. 4 (2021) 2886–2906.
DOI: https://doi.org/10.1021/acsabm.0c01640
[64] S. Sethi, B.S. Kaith, A review on chitosan-gelatin nanocomposites: synthesis, characterization and biomedical applications, React. Funct. Polym. 179 (2022) 105362.
DOI: https://doi.org/10.1016/j.reactfunctpolym.2022.105362
[65] F. Mushtaq, A. Raza, N. Ghauri, M. Zafar, M. Agib, Z. Ilyas, M. Ikram, Preparation, properties, and applications of gelatin-based hydrogels (GHs) in the environmental, technological, and biomedical sectors, Int. J. Biol. Macromol. 218 (2022) 601–633.
DOI: https://doi.org/10.1016/j.ijbiomac.2022.07.168

[66] A. Sadi, H. Ferfera-Harrar, Crosslinked CMC/gelatin bio-nanocomposite films with organoclay, red cabbage anthocyanins and pistacia leaves extract as active intelligent food packaging: colorimetric pH indication, antimicrobial/antioxidant properties, and shrimp spoilage tests, Int. J. Biol. Macromol. 242 (2023) 124964.
DOI: https://doi.org/10.1016/j.ijbiomac.2023.124964
[67] D. Kim, J. Lee, G. Kim, Biomimetic gelatin/HA biocomposites with effective elastic properties and 3D-structural flexibility using a 3D-printing process, Addit. Manuf. 36 (2020) 101616.
DOI: https://doi.org/10.1016/j.addma.2020.101616
[68] S. Nagarajan, A. Belaid, C. Radhakrishnan, E. Teyssier, V. Balvay, N. Belaid, D. Hartmann, C. Marquette, Sacrificial mold-assisted 3D printing of stable biocompatible gelatin scaffolds, Bioprinting 22 (2021) e00140.
DOI: https://doi.org/10.1016/j.bprint.2021.e00140
[69] R. Surolia, A. Singh, Pectin—structure, specification, production, applications and various emerging sources: a review, in: Sustainable Food Systems (Volume II), Springer, 2023, pp. 267–282.
DOI: https://doi.org/10.1007/978-3-031-46046-3_12
[70] M. Gavahian, A. Mousavi Khaneghah, Pectin from food processing by-products: extraction, purification, characterization, and applications, Trends Food Sci. Technol. 115 (2021) 42–54.
DOI: https://doi.org/10.1016/j.tifs.2021.06.033
[71] L. Choopani, H.A.M. Aliabadi, F. Ganjali, A. Kashtiaray, R. Eivazzadeh-Keihan, A. Maleki, M. Salimibani, A.H. Karimi, M. Mahdavi, Fabrication of a magnetic nanocomposite based on natural hydrogel: pectin, tragacanth gum, silk fibroin, and integrated graphitic carbon nitride for hyperthermia and biological features, Carbohydr. Polym. Technol. Appl. 7 (2024) 100495.
DOI: https://doi.org/10.1016/j.carpta.2024.100495
[72] P. Sapuła, K. Bialik-Wąs, K. Malarz, Are natural compounds a promising alternative to synthetic crosslinking agents in the preparation of hydrogels?, Pharmaceutics 15 (2023) 253.
DOI: https://doi.org/10.3390/pharmaceutics15010253
[73] H. Yu, Y. Liu, L. Yang, S. Zhang, Y. Zhou, H. Shi, Vanillin crosslinked chitosan/gelatin bio-polymer film with antioxidant, water resistance and ultraviolet-proof properties, Int. J. Biol. Macromol. 253 (2023) 126726.
DOI: https://doi.org/10.1016/j.ijbiomac.2023.126726
[74] G. Cavallaro, S. Milioto, S. Konnova, S. Fakhrullina, R. Fakhrullin, L. Lazzara, Chitosan-based smart hybrid materials: a physico-chemical perspective, J. Mater. Chem. B 9 (2021) 594–611.
DOI: https://doi.org/10.1039/D0TB01883A
[75] J. Wang, Y. Wang, Y. Li, W. Zhang, H. Wang, L. Wang, An injectable, dual crosslinkable hybrid pectin methacrylate (PECMA)/gelatin methacryloyl (GelMA) hydrogel for skin hemostasis applications, Int. J. Biol. Macromol. 185 (2021) 441–450.
DOI: https://doi.org/10.1016/j.ijbiomac.2021.06.135
[76] F. Abi-Ghaida, The serendipitous integration of small boron-embedded molecules into medicinal chemistry, in: Fundamentals and Applications of Boron Chemistry, Elsevier, 2022, pp. 321–410.
DOI: https://doi.org/10.1016/B978-0-12-822127-3.00005-2
[77] J. Koshy, D. Sangeetha, Recent progress and treatment strategy of pectin polysaccharide based tissue engineering scaffolds in cancer therapy, wound healing and cartilage regeneration, Int. J. Biol. Macromol. 238 (2023) 124183.
DOI: https://doi.org/10.1016/j.ijbiomac.2023.124183
[78] M. Naghdi, H. Jaleh, M. Ghanbari, M. Shahbazi, Magnetic nanostructures in nanomedicine revolution: a review of growing magnetic nanocomposites in biomedical applications, Adv. Colloid Interface Sci. 308 (2022) 102771.
DOI: https://doi.org/10.1016/j.cis.2022.102771
[79] S. Taghizadeh, N. Naderi, M. Gholipourmalekabadi, M. Ghanbari, Magnetic hydrogel applications in articular cartilage tissue engineering, J. Biomed. Mater. Res. A 111 (2023) 1709–1721.
DOI: https://doi.org/10.1002/jbm.a.37573
[80] Z. Edis, S. Wang, M.K. Bloukh, H. Işık, M. Demir Pektas, M. Taj Muhammad, Nanocarriers-mediated drug delivery systems for anticancer agents: an overview and perspectives, Int. J. Nanomed. 16 (2021) 1313–1330.
DOI: https://doi.org/10.2147/IJN.S289443
[81] S. Saadat, D. Rawtani, G. Parikh, Clay minerals-based drug delivery systems for anti-tuberculosis drugs, J. Drug Deliv. Sci. Technol. 70 (2022) 103755.
DOI: https://doi.org/10.1016/j.jddst.2022.103755
[82] E.D. Pereira, D.V. Cesar, F.G. de Souza, Study of controlled release of ibuprofen magnetic nanocomposites, J. Mol. Struct. 1232 (2021) 130067.
DOI: https://doi.org/10.1016/j.molstruc.2021.130067
[83] H.Y. Atay, Magnetic polymer nanocomposites: manufacturing and biomedical applications, in: Polymeric and Natural Composites, Springer, 2022, pp. 187–212.
DOI: https://doi.org/10.1007/978-3-030-70266-3_7
[84] B. Socas-Rodríguez, J. Hernández-Borges, M. Ángeles Herrera-Herrera, M. Ángel Rodríguez-Delgado, Recent applications of magnetic nanoparticles in food analysis, Processes 8 (2020) 1140.
DOI: https://doi.org/10.3390/pr8091140

[85] X. Yu, H. Yu, Y. Guo, Design, preparation, and application of magnetic nanoparticles for food safety analysis: a review of recent advances, J. Agric. Food Chem. 70 (2021) 46–62.
DOI: https://doi.org/10.1021/acs.jafc.1c05477
[86] H. Seo, K. Kim, S. Kim, H. Park, M. Kim, Smart contact lenses as wearable ophthalmic devices for disease monitoring and health management, Chem. Rev. 123 (2023) 11488–11558.
DOI: https://doi.org/10.1021/acs.chemrev.3c00247
[87] X. Huang, Q. Li, Y. Liu, X. Zhang, J. Wang, X. Zhang, Novel magnetic Fe3O4/α-FeOOH nanocomposites and their enhanced mechanism for tetracycline hydrochloride removal in the visible photo-Fenton process, ACS Omega 6 (2021) 9095–9103.
DOI: https://doi.org/10.1021/acsomega.1c00370
[88] L. Mohammadi, A. Rahdar, M. Khaksefidi, H. Sobhi, A. Sadeghfar, Polystyrene magnetic nanocomposites as antibiotic adsorbents, Polymers 12 (2020) 1313.
DOI: https://doi.org/10.3390/polym12061313
[89] G. Fadillah, I.M. Yola, T.A. Saleh, Magnetic iron oxide/clay nanocomposites for adsorption and catalytic oxidation in water treatment applications, Open Chem. 18 (2020) 1148–1166.
DOI: https://doi.org/10.1515/chem-2020-0179
[90] A. Babakhani, S.J. Peighambardoust, A. Olad, Fabrication of magnetic nanocomposites scaffolds based on polyvinyl alcohol-chitosan containing hydroxyapatite and clay modified with graphene oxide: evaluation of their properties for bone tissue engineering applications, J. Mech. Behav. Biomed. Mater. 147 (2023) 106263.
DOI: https://doi.org/10.1016/j.jmbbm.2023.106263
[91] T. Ahamad, M. Naushad, S.M. Alshehri, Preparation of chitosan based magnetic nanocomposite for tetracycline adsorption: kinetic and thermodynamic studies, Int. J. Biol. Macromol. 147 (2020) 258–267.
DOI: https://doi.org/10.1016/j.ijbiomac.2020.01.025
[92] W. Zhao, T. Yang, R. Wang, X. Liang, Preparation and characteristics of a magnetic carbon nanotube adsorbent: its efficient adsorption and recoverable performances, Sep. Purif. Technol. 257 (2021) 117917.
DOI: https://doi.org/10.1016/j.seppur.2020.117917
[93] S. Bosu, N. Rajamohan, M. Rajasimman, Enhanced remediation of lead(II) and cadmium(II) ions from aqueous media using porous magnetic nanocomposites—a comprehensive review on applications and mechanism, Environ. Res. 213 (2022) 113720.
DOI: https://doi.org/10.1016/j.envres.2022.113720
[94] M.K. Seliem, M. Barczak, S. Anastopoulos, A. Giannakoudakis, A novel nanocomposite of activated serpentine mineral decorated with magnetic nanoparticles for rapid and effective adsorption of hazardous cationic dyes: kinetics and equilibrium studies, Nanomaterials 10 (2020) 684.
DOI: https://doi.org/10.3390/nano10040684
[95] R. Nicola, M. Lupea, I. Atkinson, M. Voicescu, C. Socaciu, M. Baia, L. Baia, Mesoporous magnetic nanocomposites: a promising adsorbent for the removal of dyes from aqueous solutions, J. Porous Mater. 27 (2020) 413–428.
DOI: https://doi.org/10.1007/s10934-019-00823-w
[96] A. Elhambakhsh, P. Keshavarz, Investigation of carbon dioxide absorption using different functionalized Fe3O4 magnetic nanoparticles, Energy Fuels 34 (2020) 7198–7208.
DOI: https://doi.org/10.1021/acs.energyfuels.0c00715
[97] S. Pandey, A. Do, S. Sonwani, B. Ganesan, T. Aryal, R. Singh, R. Bhardwaj, Locust bean gum-based hydrogels embedded magnetic iron oxide nanoparticles nanocomposite: advanced materials for environmental and energy applications, Environ. Res. 214 (2022) 114000.
DOI: https://doi.org/10.1016/j.envres.2022.114000
[98] F. Gang, S. Zhang, A. Wang, Y. Li, H. Sun, Multifunctional magnetic hydrogel: design strategies and applications, Nano Sel. 2 (2021) 2291–2307.
DOI: https://doi.org/10.1002/nano.202100023
[99] L. Choopani, A. Mohammadi, H.A.M. Aliabadi, A. Kashtiaray, R. Eivazzadeh-Keihan, A. Maleki, M. Mahdavi, Functionalization of zinc ferrites nanoparticles by cyclic aromatic polyimide chains as a novel star polymer with antibacterial activity and low toxicity, J. Ind. Eng. Chem. (2024).
DOI: https://doi.org/10.1016/j.jiec.2024.01.047
[100] A.H.A. Hoseini, S. Asl, A. Bohloul, S. Mohammad, A.R. Zolriasatein, Synthesis of soybean-derived porous carbon as selenium host for high-performance lithium-selenium batteries, Electrochim. Acta 429 (2022) 140954.
DOI: https://doi.org/10.1016/j.electacta.2022.140954
[101] P. Pramanik, S. Koner, A. Chatterjee, A. Saha, B. Das, High surface area porous carbon from cotton stalk agro-residue for CO2 adsorption and study of techno-economic viability of commercial production, J. CO2 Util. 45 (2021) 101450.
DOI: https://doi.org/10.1016/j.jcou.2020.101450
[102] T. Shimizu, W. Ding, N. Kameta, Soft-matter nanotubes: a platform for diverse functions and applications, Chem. Rev. 120 (2020) 2347–2407.
DOI: https://doi.org/10.1021/acs.chemrev.9b00509
[103] Y. Li, T. Wang, N. Wang, J. He, Y. Liu, Y. Wang, L. Zhang, H. Sun, Manipulation of the halloysite clay nanotube lumen for environmental remediation: a review, Environ. Sci.: Nano 9 (2022) 841–866.
DOI: https://doi.org/10.1039/D1EN00893B

[104] D. Tunega, A. Zaoui, Mechanical and bonding behaviors behind the bending mechanism of kaolinite clay layers, J. Phys. Chem. C 124 (2020) 7432–7440.
DOI: https://doi.org/10.1021/acs.jpcc.0c01047
[105] J.R. Beryl, J.R. Xavier, Halloysite for clay–polymer nanocomposites: effects of nanofillers on the anti-corrosion, mechanical, microstructure, and flame-retardant properties—a review, J. Mater. Sci. 58 (2023) 10943–10974.
DOI: https://doi.org/10.1007/s10853-023-08701-2
[106] S.B.M. Khalith, M. Ravindran, V. Arasu, N. Al-Dhabi, K. Vijayaraghavan, Nanostructured catalytic membranes for water filtration, in: Nano-Bioremediation: Fundamentals and Applications, Elsevier, 2022, pp. 389–412.
DOI: https://doi.org/10.1016/B978-0-12-823962-9.00014-0
[107] A. Glotov, A. Stavitskaya, Y. Vinokurov, E. Ivanov, V. Zolotarevsky, V. Nurmukhametov, Y. Lvov, Clay nanotube-metal core/shell catalysts for hydroprocesses, Chem. Soc. Rev. 50 (2021) 9240–9277.
DOI: https://doi.org/10.1039/D1CS00201B
[108] C. Cheng, T. Song, Y. Wang, Z. Wang, X. Ma, H. Wang, L. Zhang, Halloysite nanotubes in polymer science: purification, characterization, modification and applications, Nanotechnol. Rev. 9 (2020) 323–344.
DOI: https://doi.org/10.1515/ntrev-2020-0024
[109] N. Danyliuk, J. Tomaszewska, T. Tatarchuk, Halloysite nanotubes and halloysite-based composites for environmental and biomedical applications, J. Mol. Liq. 309 (2020) 113077.
DOI: https://doi.org/10.1016/j.molliq.2020.113077
[110] S. Ata, F. Imtiaz, M. Farooq, A. Ghafoor, M. Din, Kinetics of methylene blue dye adsorptive removal using halloysite nanocomposite hydrogels, Z. Phys. Chem. 236 (2022) 373–385.
DOI: https://doi.org/10.1515/zpch-2021-3119
[111] L. Li, F. Wang, Y. Lv, J. Liu, D. Zhang, Z. Shao, Halloysite nanotubes and Fe3O4 nanoparticles enhanced adsorption removal of heavy metal using electrospun membranes, Appl. Clay Sci. 161 (2018) 225–234.
DOI: https://doi.org/10.1016/j.clay.2018.04.030
[112] S. Erdem, M. Öztekin, Y.S. Açıkel, Investigation of tetracycline removal from aqueous solutions using halloysite/chitosan nanocomposites and halloysite nanotubes/alginate hydrogel beads, Environ. Nanotechnol. Monit. Manage. 16 (2021) 100576.
DOI: https://doi.org/10.1016/j.enmm.2021.100576
[113] E. Türkeş, Y.S. Açıkel, Synthesis and characterization of magnetic halloysite–chitosan nanocomposites: use in the removal of methylene blue in wastewaters, Int. J. Environ. Sci. Technol. 17 (2020) 1281–1294.
DOI: https://doi.org/10.1007/s13762-019-02549-3
[114] U. Yildiz, Ö.F. Kemik, B. Hazer, The removal of heavy metal ions from aqueous solutions by novel pH-sensitive hydrogels, J. Hazard. Mater. 183 (2010) 521–532.
DOI: https://doi.org/10.1016/j.jhazmat.2010.07.055
[115] S.S. Mosavi, F. Ganjali, M. Heydari, A. Maleki, Magnetic carboxymethyl gond katira-grafted-poly(3-aminobenzoic acid) as an antibacterial biosorbent for purification of acetamiprid-contaminated water, Int. J. Biol. Macromol. 263 (2024) 133189.
DOI: https://doi.org/10.1016/j.ijbiomac.2024.133189
[116] Y. Ji, F. Xu, W. Wei, H. Gao, K. Zhang, G. Zhang, Y. Xu, P. Zhang, Efficient and fast adsorption of methylene blue dye onto a nanosheet MFI zeolite, J. Solid State Chem. 295 (2021) 121917.
DOI: https://doi.org/10.1016/j.jssc.2020.121917
[117] M. Topuz, Investigation of halloysite nanotube effect in poly(lactic acid)/hydroxyapatite coatings on Ti–6Al–4V biomedical alloy, J. Polym. Environ. (2023) 1–15.
DOI: https://doi.org/10.1007/s10924-023-02940-9
[118] H. Dogari, F. Ganjali, A. Maleki, M. Heydari, Magnetic polyacrylonitrile-melamine nanoadsorbent (PAN-Mel@Fe3O4) for effective adsorption of Cd(II) and Pb(II) from aquatic area, Mater. Sci. Eng.: B 298 (2023) 116871.
DOI: https://doi.org/10.1016/j.mseb.2023.116871
[119] B. Dery, L. Zaixiang, Scanning electron microscopy (SEM) as an effective tool for determining the morphology and mechanism of action of functional ingredients, Food Rev. Int. 39 (2023) 2007–2026.
DOI: https://doi.org/10.1080/87559129.2021.1934004
[120] V.G. Baldovino-Medrano, V. Niño-Celis, R.I. Giraldo, Systematic analysis of the nitrogen adsorption–desorption isotherms recorded for a series of materials based on microporous–mesoporous amorphous aluminosilicates using classical methods, J. Chem. Eng. Data 68 (2023) 2512–2528.
DOI: https://doi.org/10.1021/acs.jced.3c00142
[121] M.T. Amin, A.A. Alazba, M. Shafiq, Successful application of eucalyptus camdulensis biochar in the batch adsorption of crystal violet and methylene blue dyes from aqueous solution, Sustainability 13 (2021) 3600.
DOI: https://doi.org/10.3390/su13073600
[122] S.D.K. Seera, D.K. Kumar, T. Gopinath, P. Naik, Synthesis and characterization of xylan-gelatin crosslinked reusable hydrogel for the adsorption of methylene blue, Carbohydr. Polym. 256 (2021) 117520.
DOI: https://doi.org/10.1016/j.carbpol.2020.117520
[123] R. Ahmad, K. Ansari, Enhanced sequestration of methylene blue and crystal violet dye onto green synthesis of pectin modified hybrid (Pect/AILP-Kal) nanocomposite, Process Biochem. 111 (2021) 132–143.
DOI: https://doi.org/10.1016/j.procbio.2021.10.022

[124] B. Hastuti, S.N. Afifah, B. Mulyani, E. Susilowati, Adsorption of methylene blue dyes using pectin membrane, J. Phys.: Conf. Ser. 1567 (2020) 042068.
DOI: https://doi.org/10.1088/1742-6596/1567/4/042068
[125] J. Ren, Y. Wang, Y. Li, Y. Yao, Y. Wang, Effective removal of dyes from aqueous solutions by a gelatin hydrogel, J. Polym. Environ. 29 (2021) 3989–3999.
DOI: https://doi.org/10.1007/s10924-021-02173-8
[126] A.K. Sharma, N. Priya, A. Dohare, M. Kumari, Environmentally benign approach for the efficient sequestration of methylene blue and coomassie brilliant blue using graphene oxide emended gelatin/κ-carrageenan hydrogels, Int. J. Biol. Macromol. 219 (2022) 353–365.
DOI: https://doi.org/10.1016/j.ijbiomac.2022.08.002
[127] J. Ren, Y. Wang, Y. Yao, Y. Wang, Y. Fei, Double network gelatin/chitosan hydrogel effective removal of dyes from aqueous solutions, J. Polym. Environ. 30 (2022) 2007–2021.
DOI: https://doi.org/10.1007/s10924-021-02336-7
[128] Y. Wang, T. Chen, X. Zhang, T. Mwamulima, Removal study of crystal violet and methylene blue from aqueous solution by activated carbon embedded zero-valent iron: effect of reduction methods, Front. Environ. Sci. 9 (2021) 799264.
DOI: https://doi.org/10.3389/fenvs.2021.799264
[129] A.K. Kodoth, V. Badalamoole, Pectin based graft copolymer–ZnO hybrid nanocomposite for the adsorptive removal of crystal violet, J. Polym. Environ. 27 (2019) 2040–2053.
DOI: https://doi.org/10.1007/s10924-019-01495-y
[130] R.H. Moghaddam, A.M.H. Shabani, S. Dadfarnia, Synthesis of new hydrogels based on pectin by electron beam irradiation with and without surface modification for methylene blue removal, J. Environ. Chem. Eng. 7 (2019) 102919.
DOI: https://doi.org/10.1016/j.jece.2019.102919